


# Research of caged dynamics of clusters center atoms in $Pd_{82}Si_{18}$ amorphous alloy

Yong-He Deng(邓永和), Bei Chen(陈贝), Qing-Hua Qi(祁清华), Bing-Bing Li(李兵兵), Ming Gao(高明), Da-Dong Wen(文大东), Xiao-Yun Wang(王小云), and Ping Peng(彭平)

**Citation:**Chin. Phys. B, 2024, 33 (**4**): 047102. DOI: 10.1088/1674-1056/ad1d4e
Journal homepage: http://cpb.iphy.ac.cn; http://iopscience.iop.org/cpb

**What follows is a list of articles you may be interested in**

---

## Predicting novel atomic structure of the lowest-energy $Fe_nP_{13-n}$ ($n$=0-13) clusters: A new parameter for characterizing chemical stability

Yuanqi Jiang(蒋元祺) and Ping Peng(彭平)
Chin. Phys. B, 2023, 32 (**4**): 047102. DOI: 10.1088/1674-1056/acae75

## Plasmonic hybridization properties in polyenes octatetraene molecules based on theoretical computation

Nan Gao(高楠), Guodong Zhu(朱国栋), Yingzhou Huang(黄映洲), and Yurui Fang(方蔚瑞)
Chin. Phys. B, 2023, 32 (**3**): 037102. DOI: 10.1088/1674-1056/ac891c

## Theoretical study of $M_6X_2$ and $M_6XX'$ structure ($M$ = Au, Ag; $X$,$X'$ = S, Se): Electronic and optical properties, ability of photocatalytic water splitting, and tunable properties under biaxial strain

Jiaqi Li(李嘉琪), Xinlu Cheng(程新路), and Hong Zhang(张红)
Chin. Phys. B, 2022, 31 (**9**): 097101. DOI: 10.1088/1674-1056/ac6580

## First-principles calculations of K-shell x-ray absorption spectra for warm dense ammonia

Zi Li(李孜), Wei-Jie Li(李伟节), Cong Wang(王聪), Dafang Li(李大芳), Wei Kang(康炜), Xian-Tu He(贺贤土), and Ping Zhang(张平)
Chin. Phys. B, 2021, 30 (**5**): 057102. DOI: 10.1088/1674-1056/abdb1b

## Structural evolution and magnetic properties of $ScLi_n$ ($n$=2-13) clusters: A PSO and DFT investigation

Lu Li(栗潞), Xiu-Hua Cui(崔秀花), Hai-Bin Cao(曹海宾), Yi Jiang(姜轶), Hai-Ming Duan(段海明), Qun Jing(井群), Jing Liu(刘静), Qian Wang(王倩)
Chin. Phys. B, 2020, 29 (**7**): 077101. DOI: 10.1088/1674-1056/ab8d9e

---

# Research of caged dynamics of clusters center atoms in $Pd_{82}Si_{18}$ amorphous alloy

Yong-He Deng(邓永和)[1,†], Bei Chen(陈贝)[2], Qing-Hua Qi(祁清华)[2], Bing-Bing Li(李兵兵)[2], Ming Gao(高明)[1], Da-Dong Wen(文大东)[1], Xiao-Yun Wang(王小云)[2,‡], and Ping Peng(彭平)[3]

[1] *School of Computational Science and Electronics, Hunan Institute of Engineering, Xiangtan* 411104, *China*
[2] *School of Physics and Mechanical & Electrical Engineering, Jishou University, Jishou* 416000, *China*
[3] *School of Materials Science and Engineering, Hunan University, Changsha* 410082, *China*

(Received 14 December 2023; revised manuscript received 8 January 2024; accepted manuscript online 11 January 2024)

To date, there is still a lack of a comprehensive explanation for caged dynamics which is regarded as one of the intricate dynamic behaviors in amorphous alloys. This study focuses on $Pd_{82}Si_{18}$ as the research object to further elucidate the underlying mechanism of caged dynamics from multiple perspectives, including the cage's lifetime, atomic local environment, and atomic potential energy. The results reveal that Si atoms exhibit a pronounced cage effect due to the hindrance of Pd atoms, resulting in an anomalous peak in the non-Gaussian parameters. An in-depth investigation was conducted on the caged dynamics differences between fast and slow Si atoms. In comparison to fast Si atoms, slow Si atoms were surrounded by more Pd atoms and occupied lower potential energy states, resulting in smaller diffusion displacements for the slow Si atoms. Concurrently, slow Si atoms tend to be in the centers of smaller clusters with coordination numbers of 9 and 10. During the isothermal relaxation process, clusters with coordination numbers 9 and 10 have longer lifetimes, suggesting that the escape of slow Si atoms from their cages is more challenging. The findings mentioned above hold significant implications for understanding the caged dynamics.

**Keywords:** caged dynamics, $Pd_{82}Si_{18}$ amorphous alloy, fast and slow atoms, clusters, lifetime

**PACS:** 71.15.Pd, 64.70.pe, 61.25.Mv, 64.70.D– **DOI:** 10.1088/1674-1056/ad1d4e

## 1. Introduction

Amorphous alloy is a new type of metal material that is obtained by using the rapid solidification technology of metallurgy and the concept of entropy control to suppress the crystallization of alloy melt and maintain the disordered structure of the melt,[1] which has attracted increasing attention because of its unique physical and chemical properties.[2–4] The microstructure and dynamic behavior of amorphous alloys have always been the focus of research, studying the dynamic behavior of amorphous alloys can reveal the formation process and structural evolution mechanism. A large number of experiments and simulation results showed that the microstructure of amorphous alloys is heterogeneous.[5–7] The relaxation behavior of amorphous alloys is a macroscopic manifestation of microstructural heterogeneity in response to external thermal stimulation.[8] A consensus regarding the atomic motion mechanism within glass has been reached based on molecular dynamics simulations, during quenching, the transport properties of a glass-forming liquid exhibit a dynamical crossover from Arrhenius to super-Arrhenius behavior.[9,10] The Arrhenius crossover temperature $T_A$ marks the onset of spatial heterogeneity correlated with dynamics.[11] During the transition from liquid to amorphous, numerous cluster structures are formed and atoms are trapped within these clusters, which is known as the cage effect.[12] When the undercooled liquid is cooled below $T_g$, liquid-like motions freeze and atomic mobility becomes gradually constrained by neighbor atoms. Consequently, caged dynamics below $T_g$ become more pronounced. Atoms' escape from their cages necessitates overcoming barriers associated with the collective rearrangement of neighboring atoms to create free space.[13] Studies on single-atom dynamics in glasses have revealed that both bulk and surface dynamics exhibit Arrhenius behavior dominated by caging and hopping motions.[14] The duration of caged dynamics is shorter than $\beta$ relaxation but longer than the boson peak, resulting in nearly constant dielectric and mechanical magnetization loss.[15–17]

In the field of metallic glasses, there is still a lack of a comprehensive explanation for the specific dynamic behavior, as well as its impact on mechanical and physical properties with other relaxations.[18] Previous research on various metal glasses using different experimental techniques has revealed that caged dynamics terminates before the onset of $\beta$-relaxation at low frequencies, indicating a coupling between these two processes where certain attributes of one process can be transferred or reflected in the other.[19–21] Therefore, studying caged dynamics is crucial for understanding $\beta$-relaxation.

Caged dynamics play a crucial role in influencing the glass transition, deformation behavior under stress, and sta-

†Corresponding author. E-mail: dengyonghe1@163.com
‡Corresponding author. E-mail: wxyyun@163.com

© 2024 Chinese Physical Society and IOP Publishing Ltd 

bility of amorphous structures during annealing and processing, which are essential for understanding and predicting the mechanical, thermal, and physical properties of amorphous alloys.[22] $Pd_{82}Si_{18}$ alloy with a deep eutectic composition is a typical material for studying the formation and properties of amorphous alloys.[23–25] Due to significant differences in atomic size and chemical properties between eutectic alloys compared to single-phase alloys, eutectic alloys exhibit more complex dynamic behaviors.[26] Therefore, this study selects $Pd_{82}Si_{18}$ as the research subject to reveal the mechanism of caged dynamics from the perspectives of differences between fast and slow atoms and the cage's lifetime.

## 2. Method

LAMMPS (large-scale atomic molecular massively parallel simulator) was used to simulate the rapid solidification process of $Pd_{82}Si_{18}$ liquid alloy at 0 GPa. $5\times10^4$ atoms ($4.1\times10^4$ Pd atoms and $9\times10^3$ Si atoms) were randomly placed in a cubic box, and each atom was assigned an identity document. The numerical integration of atomic motion employed the Verlet[27] velocity algorithm, and the time step used to integrate the equations of motion is chosen as 2 fs. The embedded-atom method (EAM) potential was used to describe the interactions between atoms.[28] Firstly, the system was allowed to relax at a constant temperature of 2100 K for $1\times10^6$ steps (2 ns) to achieve melting and equilibrium. Subsequently, the temperature was decreased at a cooling rate of $10^{11}$ K/s to the temperature of interest. Finally, each system was allowed to relax at the constant temperature of interest for 10 ps. With recordings of temperature, atomic coordinates, potential energy, and other information every 5 steps.

## 3. Results and discussion

Mean square displacement (MSD) describes the deviation of the particle's movement from a reference position over time, serving to characterize the diffusion behavior and mechanisms of particles. The calculation formula of MSD is as follows:

$$\left\langle \Delta r^2(t)\right\rangle = \left\langle \frac{1}{N}\sum_{j=1}^{N}\left|\boldsymbol{r}_j(t+t_0)-\boldsymbol{r}_j(t_0)\right|^2\right\rangle, \tag{1}$$

where $r_j(t_0)$ is the position of the particle at the initial time, $r_j(t+t_0)$ is the position of the particle after a period of time $t$, and $\langle\cdot\rangle$ donates the ensemble average.

The utilization of non-Gaussian parameters (NGP) enables the investigation of the dynamic non-uniformity of the system. The corresponding formula is outlined as follows:

$$\alpha_2(t) = \frac{3\left\langle r^4(t)\right\rangle}{5\left\langle r^2(t)\right\rangle^2} - 1, \tag{2}$$

where $\left\langle r^2(t)\right\rangle$ is the MSD of the system, and the $\alpha_2(t)$ indicates the degree of deviation from the Gaussian distribution. It is frequently employed to delineate the kinetic behavior of amorphous materials.

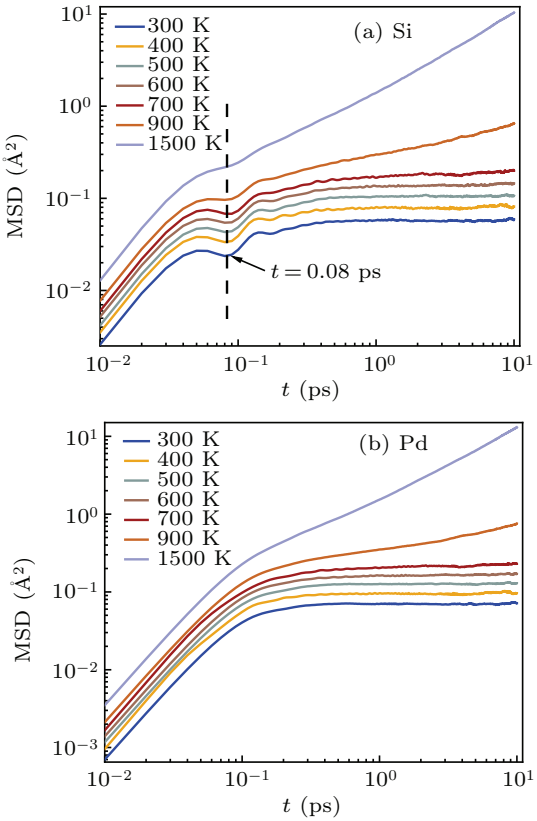



**Fig. 1.** The variation of the mean square displacement with time during isothermal relaxation at different temperatures: (a) Si atoms and (b) Pd atoms.

According to the literature,[29] the glass transition temperature of $Pd_{82}Si_{18}$ was approximately 730 K when the rapid solidification process was simulated by the molecular dynamics method. $Pd_{82}Si_{18}$ that rapidly solidified to 1500 K is in a melt state; when rapidly solidified to 900 K, it becomes an undercooled liquid and upon further cooling, transitions to the solid phase. To explore the caged dynamics of the system before the $\beta$-relaxation occurred, isothermal relaxation was performed at different temperatures. Figure 1 shows the MSD of Pd and Si atoms in the $Pd_{82}Si_{18}$ amorphous alloy system during isothermal relaxation at different temperatures. The MSD exhibits the expected ballistic behavior with a short period of time, atoms can move unhindered within clusters, and the MSD curve shows almost linear growth. When atomic movement is constricted by the surrounding atoms, the diffusion is hindered, leading to a decline in the slope of the MSD curve, this phenomenon known as the cage effect, has been extensively documented in the scientific literature. $\beta$-relaxation occurs after the atoms break the cages. It can be observed from Fig. 1(b) that Pd atoms are not confined within the cages, to put it another way, they rapidly break their cages and first participate in $\beta$-relaxation, thereby making a significant contribution to $\beta$-relaxation of the system. However, Si atoms experience a robust cage effect before 0.08 ps; the onset of $\beta$-relaxation

of Si atoms occurs when their cages are disrupted. Pd and Si atoms in $Pd_{82}Si_{18}$ amorphous alloys demonstrate different caged dynamics during isothermal relaxation. It can also be observed from Fig. 1 that as the temperature decreases, the cage effect of Si atoms becomes more obvious, the cage effect of Si atoms is most prominent in the solid $Pd_{82}Si_{18}$ alloy at 300 K.

Figure 2 depicts the temporal evolution of NGP for Pd atoms and Si atoms during the isothermal relaxation of $Pd_{82}Si_{18}$ alloy at 300 K. The $\alpha_2(t)$ of Si atoms shows an abnormal peak at 0.08 ps in Fig. 2, indicating that the motion of Si atoms is heterogeneous. The diffusion of Pd atoms conforms to the evolution law of atoms that in most systems;[30] the value tends to zero within a brief interval, reaching a peak over time; as time progresses further, the curve gradually decays from the peak value to zero. It is evident that Pd atoms serve as the rapidly moving atoms, while Si atoms represent the slower ones in the $Pd_{82}Si_{18}$ alloy. Next, an in-depth analysis of the fast and slow atomic behavior of Si atoms with an anomalous Gaussian peak will be conducted to gain a comprehensive understanding of the effects of these distinct atomic motions on the dynamical heterogeneity of the system and to elucidate the correlation between caged dynamics and $\beta$-relaxation. The way to isolate fast and slow atoms is by calculating the selfpart of the time-dependent Von Hove correlation function with $\Delta t = 0.08$ ps, and the function is defined as

$$G_s(r,t) = \frac{1}{N}\left\langle \sum_{j=1}^{N} \delta(r + r_j(0) - r_j(t)) \right\rangle. \tag{3}$$

As shown in Fig. 3, identifying 10% of Si atoms as fast atoms and 10% of Si atoms as slow atoms based on atomic displacement during $\Delta t = 0.08$ ps. The fast Si atoms are those with displacement exceeding 0.2291 Å during $\Delta t$, while the slow Si atoms are those with displacement less than 0.0629 Å during $\Delta t$. It can be observed from Fig. 3 that within 0.08 ps, the displacement of Si atoms is primarily confined to a small displacement region, while the displacement of Pd atoms is predominantly situated in the large displacement region. Consequently, Pd atoms contribute significantly to the overall diffusion displacement. The time evolution of the MSD for both fast and slow Si atoms during the isothermal relaxation process at 300 K is shown in Fig. 4. Compared with fast Si atoms, slow Si atoms have a shorter ballistic region with less diffusion before experiencing cage effects. The MSD of slow Si atoms decreases significantly before 0.08 ps, and the onset of caged dynamics is also earlier than that of fast Si atoms. Due to the presence of fast atoms, even though slow atoms gradually reduce their deviation from their initial positions because of the cage effect, the fast atoms have already deviated far from their initial positions, resulting in obvious changes in the local structure of the system. From 0.08 ps onwards, the slow Si atoms randomly leap from their cages and enter the $\beta$-relaxation; this occurs concurrently with the cracking of their cages. The findings mentioned above indicate that slow Si atoms face a greater challenge in escaping their cages before $\beta$-relaxation, as they are bound by more surrounding atoms in comparison to fast Si atoms. The prominence of their caged dynamic behavior results in the emergence of local heterogeneity in the system's dynamics, and suggests a lag in the occurrence of $\beta$-relaxation for slow Si atoms.

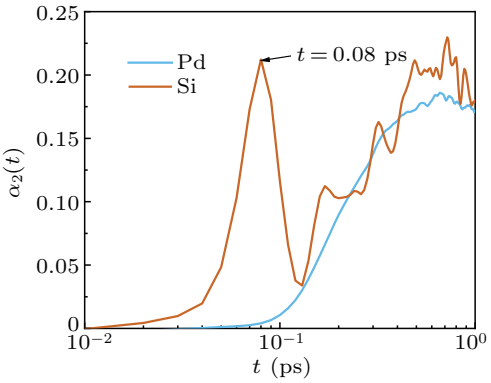



**Fig. 2.** The evolution of the non-Gaussian parameter of Pd and Si with time during the isothermal relaxation process at 300 K.

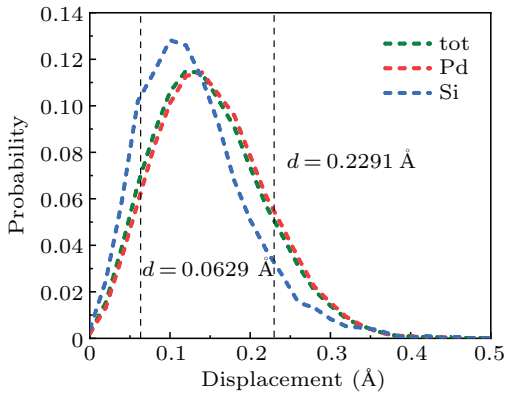



**Fig. 3.** Von Hove correlation functions of Pd, Si, and the system with $\Delta t = 0.08$ ps.

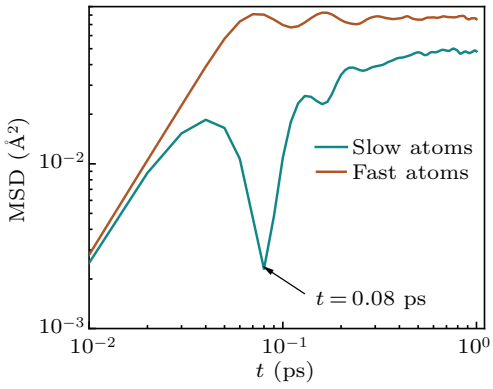



**Fig. 4.** The variation of the mean square displacement of slow and fast Si atoms with time at 300 K.

In order to investigate the correlation among dynamic behavior, relaxation, and microstructure, as well as further analyze the reasons for the pronounced cage effect experienced

by slow Si atoms, the local environment of both fast and slow Si atoms was analyzed. The radial distribution function[31] is a frequently employed technique to describe the spatial distribution of particles. It refers to selecting a particle as a reference point in the system, and then the correlation and distribution between other particles and the reference point are investigated. Figure 5 shows the partial radial distribution functions of fast and slow Si atoms to Pd atoms at the beginning of isothermal relaxation. As illustrated in Fig. 5, it can be observed that the first peak of $g_{\mathrm{Si-Pd}}(r)$ for slow Si atoms is significantly higher than that for fast Si atoms, which means that more Pd atoms are around the slow Si atoms. Figure 5 further provides the number of first nearest neighbor Pd atoms for fast and slow Si atoms which were searched with the distance of the first peak appearing. It can be seen that there are 3.2 Pd atoms around each slow Si atom ($N_{\mathrm{S}}$), while only 2.9 Pd atoms around each fast Si atom ($N_{\mathrm{F}}$). Pd atoms are larger in size compared with Si atoms, so slow Si atoms show a more pronounced cage effect than fast Si atoms. In the face of small-size Si atoms or Pd atoms of the same size, Pd atoms break through their cages more quickly, with a less pronounced cage effect. Materials tend to evolve towards low potential energy based on the principle of minimum potential energy,[32] and this also applies to relaxation and aging in amorphous materials. Figure 6 shows the relationship between the potential energy of fast and slow Si atoms over time within the range of 0 ps–1 ps. The potential energy of slow atoms is lower than that of fast atoms, with slight fluctuations observed in the former, while a clear downward trend is evident in the latter. This indicates that slow atoms are in a relatively stable state with low potential energy. However, fast atoms possess higher potential energy and are less stable, gradually evolving towards lower potential energy as time progresses.

The differences in caged dynamics of fast and slow Si atoms, along with their underlying causes, have been given a preliminary explanation. Atoms are in a specific local environment. To gain a deeper understanding of the local structure of fast and slow Si atoms, the cluster-type index method-3 (CTIM-3)[33,34] was employed to search and characterize atomic local structures. CTIM-3 is an extended cluster-type index method derived from the H–A[35] bond-type index to describe the topological structures of different atomic clusters. In this method, nine integer indexes ($N$, $n_1$, $n_2$, $n_3$, $n_4$, $n_5$, $n_6$, $n_7$, $n_8$) are assigned to denote different types of basic clusters which are defined as a group of atoms bound together with a central atom as the core surrounded by the nearest-neighbor atoms, where $N$ is the coordination number (CN), scilicet, is the number of nearest-neighbor atoms of the central atom, and $n_1$, $n_2$, $n_3$, $n_4$, $n_5$, $n_6$, $n_7$, and $n_8$ in turn denote the numbers of 1441, 1551, 1661, 1421, 1422, 1541, 1431, and 1321 bond-types. Face-centered-cubic (fcc) and body-centered-cubic (bcc) clusters can be expressed by (12 0 0 0 12 0 0 0 0) and (14 6 0 8 0 0 0 0 0).

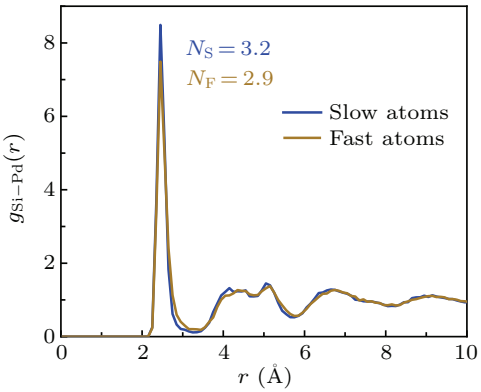



**Fig. 5.** The $g_{\mathrm{Si-Pd}}(r)$ for slow and fast Si atoms.

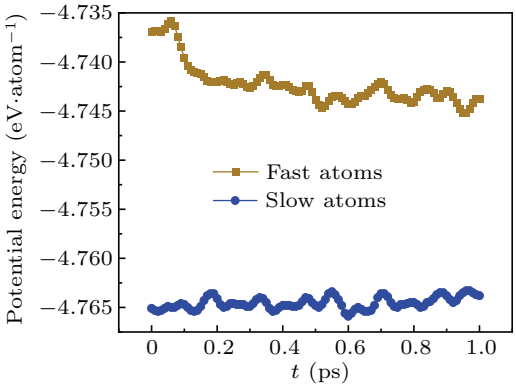



**Fig. 6.** The variation of potential energy with time of slow and fast Si atoms.

Table 1 lists the most common cluster types with fast and slow Si atoms as centers at the beginning of relaxation (0 ps) and at 0.08 ps, along with the likelihood of these cluster types possessing fast or slow atoms as their centers. The data at 0 ps and 0.08 ps in Table 1 and Table 2 exhibit similar rules as follows: Slow Si atoms are primarily located at the center of (10 2/1441 8/1551) clusters, while fast Si atoms mainly reside in the core of (11 2/1441 8/1551 1/1661) clusters. The highest probability centers on slow Si atoms cluster types are (9 1/1441 4/1551 4/1431) and (9 3/1441 6/1551), followed by (10 2/1441 8/1551); (12 2/1441 8/1551 2/1661) is the cluster with the highest probability of having a fast atom as its central atom, followed by (11 1/1441 6/1551 2/1541 2/1431) and (11 2/1441 8/1551 1/1661). In other words, slower Si atoms exhibit a greater propensity to occupy the core of clusters with lower coordination numbers (CN = 9, 10), whereas fast Si atoms are more likely to be in the center of clusters with higher coordination numbers (CN = 11, 12).

The aforementioned analysis demonstrates that slow atoms possess lower potential energy and tend to be the core of clusters with lower coordination numbers (CN = 9, 10). In comparisons, fast atoms possess higher potential energy and tend to be the core of clusters with higher coordination numbers (CN = 12, 11). How does being at the center of different clusters affect the diffusion motion and energy state of

atoms? A comprehensive analysis of several representative cluster types is conducted to elucidate this issue.

Figure 7 is the MSD of Si atoms at the center of different clusters with time, the diffusion displacement in the ballistic region is minimal for Si atoms with CN = 9, and with an increase in CN, the diffusion displacement of Si atoms in the ballistic region increases.

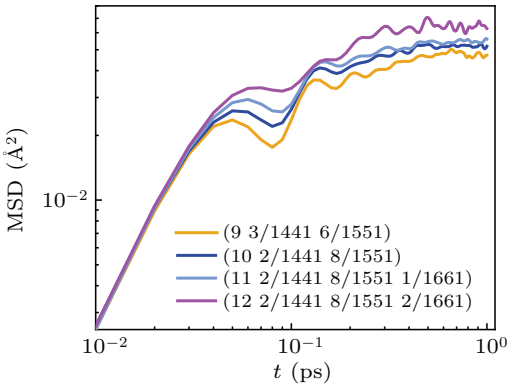



**Fig. 7.** The variation of MSD of Si atoms at the center of different clusters with time.

Figure 8 shows the average distance between the central atom and coordinating atoms in clusters with different coordination numbers, serving as a rough approximation for the radius of irregular clusters. From Fig. 8, it can be observed that the cluster radii of (9 3/1441 6/1551) and (10 2/1441 8/1551) are smaller than those of (11 2/1441 8/1551 1/1661) and (12 2/1441 8/1551 2/1661). Indicating that atoms within clusters CN = 9 and 10 have a smaller range for free motion, resulting in less displacement in the ballistic region; they are also constrained by cages earlier. Consequently, these atoms exhibit small displacements within a time frame of 0.08 ps, making them slow atoms.

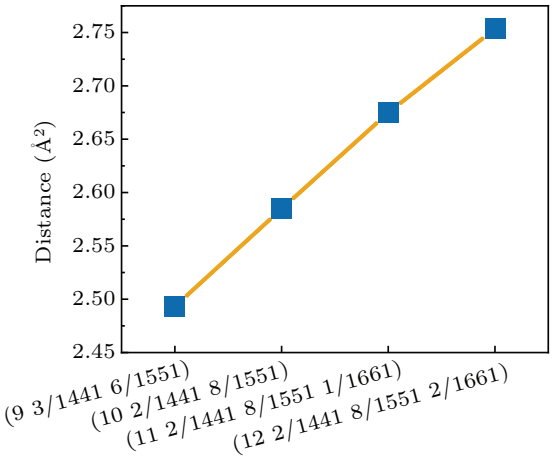



**Fig. 8.** The average distance between the center atom and the coordination atom of different clusters at 0 ps.

**Table 1.** The most common cluster types with fast and slow Si atoms as centers at the beginning of relaxation (0 ps), along with the probability of these cluster types possessing fast or slow atoms as their centers.

| Fast atoms | | | Slow atoms | | |
|---|---|---|---|---|---|
| Cluster | Number | Probability | Cluster | Number | Probability |
| (11 2/1441 8/1551 1/1661) | 125 | 0.1189 | (10 2/1441 8/1551) | 162 | 0.1153 |
| (10 2/1441 8/1551) | 108 | 0.0769 | (11 2/1441 8/1551 1/1661) | 97 | 0.0922 |
| (10 1/1441 5/1551 1/1541 3/1431) | 80 | 0.1047 | (9 1/1441 4/1551 4/1431) | 81 | 0.1375 |
| (11 1/1441 6/1551 2/1541 2/1431) | 35 | 0.1417 | (10 1/1441 5/1551 1/1541 3/1431) | 81 | 0.1060 |
| (10 3/1441 6/1551 1/1661) | 35 | 0.1080 | (9 3/1441 6/1551) | 69 | 0.1226 |
| (12 2/1441 8/1551 2/1661) | 30 | 0.1676 | (10 3/1441 6/1551 1/1661) | 28 | 0.0864 |

**Table 2.** The most common cluster types with fast and slow Si atoms as centers at the beginning of relaxation (0.08 ps), along with the probability of these cluster types possessing fast or slow atoms as their centers.

| Fast atoms | | | Slow atoms | | |
|---|---|---|---|---|---|
| Cluster | Number | Probability | Cluster | Number | Probability |
| (11 2/1441 8/1551 1/1661) | 118 | 0.1146 | (10 2/1441 8/1551) | 149 | 0.1041 |
| (10 2/1441 8/1551) | 115 | 0.0804 | (11 2/1441 8/1551 1/1661) | 96 | 0.0932 |
| (10 1/1441 5/1551 1/1541 3/1431) | 77 | 0.0997 | (9 1/1441 4/1551 4/1431) | 88 | 0.1472 |
| (10 3/1441 6/1551 1/1661) | 34 | 0.1147 | (10 1/1441 5/1551 1/1541 3/1431) | 85 | 0.1101 |
| (11 1/1441 6/1551 2/1541 2/1431) | 33 | 0.1364 | (9 3/1441 6/1551) | 79 | 0.1540 |
| (12 2/1441 8/1551 2/1661) | 32 | 0.1584 | (10 3/1441 6/1551 1/1661) | 26 | 0.0878 |

Figure 9 further shows the potential energy of these atoms, the Si atoms with CN = 9, 10 are in a relatively stable state with lower potential energy. All in all, compared with clusters with CN = 11 and 12, clusters with CN = 9 and 10 exhibit lower potential energy, smaller displacements, and are confined by smaller cages. The findings suggest that in the $Pd_{82}Si_{18}$ amorphous alloy, clusters serve as cages to confine Si atoms; the smaller the CN of Si atoms, the smaller their cages and MSD, and the lower their potential energy before $\beta$-relaxation occurs.

Since 0.08 ps, Si atoms have randomly jumped out of their cages, leading to cage disintegration and subsequent entry into $\beta$-relaxation. To investigate the lifetime of clusters during the relaxation process, the initial point was set at

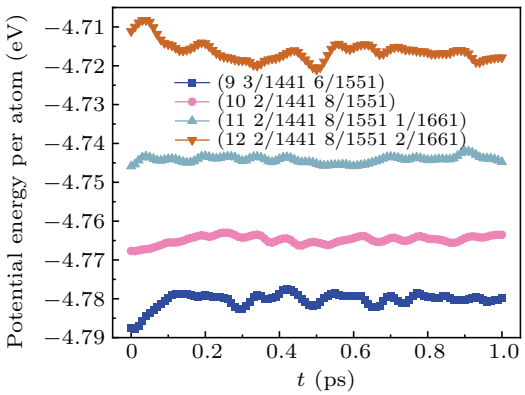



**Fig. 9.** The variation of the potential energy of Si atoms located in different cluster centers with time.

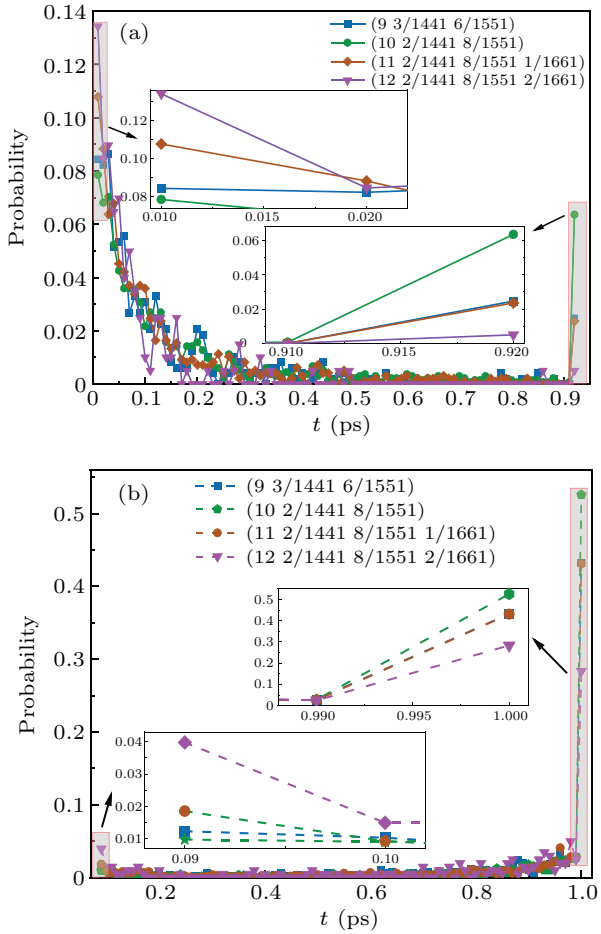



**Fig. 10.** Distribution of lifetime of different types of clusters: (a) duration of continuous existence and (b) final appearance time.

0.08 ps. The duration of continuous existence of clusters from 0.08 ps to 1 ps, as well as the time of the last appearance of clusters, were analyzed, as illustrated in Fig. 10. The former only considered the continuous existence of clusters in the relaxation process, and its duration would cease if the cluster structure changed at a certain time, the latter ignores the alterations in cluster structure during the relaxation process and instead focus on the time when the cluster last appears; this time interval is then considered as the cluster lifetime. Figure 10(a) shows the distribution of continuous existence duration. The likelihood of clusters with CN = 11 and 12 terminating within a short time is higher compared with that of clusters with CN = 9 and 10; clusters with CN = 11 and 12 exhibit a lower probability of continuous existence up to 1 ps than clusters with CN = 9 and 10. This means that the first way of exploring lifetime suggests that clusters with CN = 9 and 10 have a longer lifetime. The distribution of the time that the clusters' final appearance is shown in Fig. 10(b). On the one hand, clusters with CN = 11 and 12 have a higher probability of disappearing in a short period compared with clusters with CN = 9 and 10; on the other hand, clusters with CN = 9 and 10 have a higher probability of persisting for longer periods than clusters with CN = 11 and 12. In other words, the second method confirms that clusters with CN = 9 and 10 have longer lifetimes. The conclusions obtained by two different methods of exploring lifetime are essentially consistent. In summary, in $Pd_{82}Si_{18}$ amorphous alloy, low-coordinated (CN = 9, 10) clusters centered around Si have longer lifetimes compared with high-coordinated (CN = 12, 11) Si-centered clusters. Therefore, their cages are more difficult to break, making it harder for the confined Si atoms to escape.

## 4. Conclusion

The caged dynamics of Si atoms in $Pd_{82}Si_{18}$ amorphous alloys at low temperatures were investigated by molecular dynamics simulations. The emergence of an anomalous peak in the NGP of Si atoms was observed at 0.08 ps, and its decline signified that Si atoms escaped their cages and entered into $\beta$-relaxation. Notable disparities were observed in the caged dynamics of both fast and slow Si atoms. This was attributed to the fact that slow Si atoms, being in a state of lower potential energy, were surrounded by more large-sized Pd atoms that hindered their diffusion, thereby rendering their cages binding more robust compared with fast Si atoms, which were in a state of higher potential energy. We observed that slow Si atoms tend to be situated in the center of clusters with CN = 9 and 10, while fast Si atoms tend to be in the center of clusters with CN = 11 and 12. Slow atoms are surrounded by a higher concentration of Pd atoms and are caged by smaller clusters, resulting in less freedom of movement in the cluster, earlier onset of the cage effect, and lower potential energy. The findings reveal that the lifetime of clusters with CN = 10 and 9 is longer than that of clusters with CN = 11 and 12. This indicates that the cage-like structure of the former is more challenging to break, and the atoms in its center are more difficult to escape from the confinement. The investigation is of great significance for understanding the mechanism of caged dynamics in binary alloys and provides certain guidance for exploring the glass transformation, diffusion, and deformation of amorphous alloys.

## Acknowledgements

Project supported by the National Natural Science Foundation of China (Grant No. 51701071), the Natural Science Foundation of Hunan Province, China (Grant Nos. 2022JJ50115 and 2021JJ30179), and the Research Foundation of the Education Bureau of Hunan Province, China (Grant No. 22A0522).

## References

[1] Debenedetti P G and Stillinger F H 2001 *Nature* **410** 259
[2] Guo T Q, Hu P F, Li L D, Wang Z C and Guo L 2023 *Chem.* **9** 1080
[3] Chu F, Wu K Y, Meng Y Y, Edalati K and Lin H J 2021 *Int. J. Hydrog. Energy* **46** 25029
[4] Yang Y C, Xia Z H and Mukherjee S 2021 *Nano Lett.* **21** 9108
[5] Fan C, Kecskes L J, Qiao D C, Choo H and Liaw P K 2006 *J. Non-Cryst. Solids* **352** 174
[6] Zhang S, Chong K, Zhang Z B, Gao Y, Wu D T, Zhao G L and Zou Y 2022 *J. Non-Cryst. Solids* **593** 121775
[7] Wang F, Yuan T C, Li R D, Lin S Q, Xie Z H, Li L B, Cristino V, Xu R and Liu B 2023 *J. Alloys Compd.* **942** 169065
[8] Xu Z R, Qiao J C, Wang J, Pineda E and Crespo D 2022 *J. Mater. Sci. Technol.* **99** 39
[9] Jaiswal A, Egami T and Zhang Y 2015 *Phys. Rev. B* **91** 134204
[10] Puosi F, Jakse N and Pasturel A 2018 *J. Phys.: Condens. Matter* **30** 145701
[11] Jaiswal A, Egami T, Kelton K F, Schweizer K S and Zhang Y 2016 *Phys. Rev. Lett.* **117** 205701
[12] Lyulin A V, Vorselaars B, Mazo M A, Balabaev N K and Michels M A J 2005 *Europhys. Lett.* **71** 618
[13] Ding J, Li L, Wang N, Tian L, Asta M, Ritchie R O and Egami T 2021 *Mater. Today Phys.* **17** 100359
[14] Annamareddy A, Voyles P M, Perepezko J and Morgan D 2021 *Acta Mater.* **209** 116794
[15] Capaccioli S, Ngai K L, Ancherbak S and Paciaroni A 2012 *J. Phys. Chem. B* **116** 1745
[16] Habasaki J and Ngai K L 2006 *J. Non-Cryst. Solids* **352** 5170
[17] Chen Y X, Pan S P, Lu X Q, Kang H, Zhang Y H, Zhang M, Feng S D, Ngai K L and Wang L M 2022 *J. Non-Cryst. Solids* **590** 121699
[18] Wang W H 2019 *Prog. Mater. Sci.* **106** 100561
[19] Wang Z, Ngai K L, Wang W H and Capaccioli S 2016 *J. Appl. Phys.* **119** 024902
[20] Capaccioli S, Ngai K L, Thayyil M S and Prevosto D 2015 *J. Phys. Chem. B* **119** 8800
[21] Wang B, Zhou Z Y, Guan P F, Yu H B, Wang W H and Ngai K L 2020 *Phys. Rev. B* **102** 094205
[22] Priezjev N V 2016 *Phys. Rev. E* **93** 013001
[23] Ohkubo T and Hirotsu Y 2003 *Phys. Rev. B* **67** 094201
[24] Chen N, Li Y and Yao K F 2010 *J. Alloys Compd.* **504** S211
[25] Wang X T, Zeng M, Nollmann N, Wilde G, Wang J and Tang C Y 2017 *AIP Adv.* **7** 065206
[26] Wu B Q, Kong L T and Li J F 2021 *Acta Mater.* **207** 116705
[27] Verlet L 1967 *Phys. Rev.* **159** 98
[28] https://www.google.com/site/eampotentials/Table/PdSi
[29] Wen T Q, Wang C Z, Kramer M J, Sun Y, Ye B L, Wang H D, Liu X Y, Zhang C, Zhang F, Ho K M and Wang N 2019 *Phys. Rev. B* **100** 174101
[30] Chen Y X, Feng S D, Lu X Q, Pan S P, Xia C Q and Wang L M 2023 *J. Chem. Phys.* **158** 134511
[31] Ojovan M I and Louzguine-Luzgin D V 2020 *J. Phys. Chem. B* **124** 3186
[32] Sabaryati J, Utami L S, Hasanah A W and Viridi S 2021 *J. Phys. Conf. Ser.* **1816** 012110
[33] Liu R S, Liu H R, Dong K J, Hou Z Y, Tian Z A, Peng P and Yu A B 2009 *J. Non-Cryst. Solids* **355** 541
[34] Mo Y F, Liu R S, Tian Z A, Liang Y C, Zhang H T, Hou Z Y, Liu H R, Zhang A L, Zhou L L, Peng P and Xie Z 2015 *Physica B* **465** 81
[35] Suzuki K, Hayashi N, Tomizuka Y, Fukunaga T, Kai K and Watanabe N 1984 *J. Non-Cryst. Solids* **61** 637